Suppression of the critical angle of diffraction in thin-film colloidal photonic crystals

Sergei G. Romanov*
Institute of Optics, Information and Photonics, University of Erlangen-Nuremberg, Günther-Scharowsky-Str. 1, 91058 Erlangen, Germany and Ioffe Physical Technical Institute, Polythekhnicheskaya st., 26, 194021 St. Petersburg, Russia

Ulf Peschel
Institute of Optics, Information and Photonics, University of Erlangen-Nuremberg, Günther-Scharowsky-Str. 1, 91058 Erlangen, Germany

Maria Bardosova
Tyndall National Institute, Prospect Row, Cork, Ireland

Sabine Essig and Kurt Busch
Institut für Theoretische Festkörperphysik and DFG-Center for Functional Nanostructures (CFN), Karlsruhe Institute of Technology (KIT), 76128 Karlsruhe, Germany

(Received 20 February 2010; revised manuscript received 15 July 2010; published 3 September 2010)

We present an experimental and numerical investigation of the polarization anisotropy of the zero-order backdiffracted light from three-dimensional thin-film photonic crystals assembled from colloidal spheres. In particular, we compare simulations of reflectance spectra from perfectly ordered fcc lattice of spheres with measured reflectance data from self-organized opal films and forced-assembled Langmuir-Blodgett crystal films. We identify cross-polarization couplings and interactions between photonic crystal eigenmodes as the major physical mechanisms for resonance depolarization effects. Based on this, we find that a necessary condition for the observation of critical angles of diffraction in three-dimensional lattices is that the orientation of the light's plane of incidence coincides with a high-symmetry plane of the crystal lattice. We further show that for currently achievable colloidal photonic crystals with moderate refractive index contrast, this resonance depolarization mechanisms together with the destructive influence of lattice disorder effectively renders the meaning of a critical angle of diffraction obsolete.

DOI: 10.1103/PhysRevB.82.115403 PACS number(s): 42.70.Qs, 42.25.Fx

I. INTRODUCTION

A strong polarization dependence of the optical response is a fundamental property of photonic crystals (PhCs) and relates to the topology of the electromagnetic field.[1,2] One prominent example is the critical angle of diffraction which is defined as that angle at which the diffraction resonance under TM-polarized illumination (*p* polarization) collapses while it persists for TE-polarized light (*s* polarization). In the simple case of a Bragg mirror, this effect originates from the refraction of light at the planar interfaces between the various layers of different dielectrics and can be treated using the analogy to the Brewster angle of reflectance at the planar interface between two homogeneous media.[3]

Inside three-dimensional (3D) PhCs, where planar material interfaces are absent, TE and TM polarization are actually ill-defined polarization states of light. Instead, the polarization anisotropies of the optical properties of PhC slabs have to be defined with respect to the interfaces with the surrounding homogeneous half spaces. For instance, we can determine how much of incident polarized light is reflected or transmitted into this same and the orthogonal polarization state. This circumstance makes observed polarization anisotropies of 3D PhCs dependent on fundamental and "packaging"-related properties. The former are described by the photonic band structures (dispersion relation and structure of the associated Bloch modes) of infinite PhCs (Ref. 4) while the latter refer to size, shape, and environment of actual PhC samples. Obviously, the broad variety of packaging conditions for a given PhC structure leads to a correspondingly rich diversity of experimental observations. In addition, the imperfect nature of ordering inside "real-life" PhC lattices further affects their optical response.

Among 3D PhCs, opal-like colloidal crystals are the most frequently investigated materials. This is the result of their relative ease of preparation,[5] large sample sizes and rather spectacular transformations of their spectra upon changing the propagation direction and polarization of light.[6–10] In the past, colloidal crystals were stabilized in a liquid by electrostatic forces and possessed a lattice constant that far exceeded the diameter of a single sphere.[11] Light diffraction in such crystals is fully described by the Bragg law and Mie theory. In contrast, opal-like crystals consist of closely packed arrangements of spheres, therefore Mie resonances of individual spheres are suppressed, the diffraction resonances are significantly broadened and the resonance dispersion progressively deviates from the Bragg law when the refractive index (RI) contrast between the particles and the surrounding medium is increased. These changes are accompanied by an increasing influence of lattice defects that allow for uncoupled light to propagate across the PhCs. This leads to resonance broadening and, eventually, washes out fine features of optical spectra.

Based on this, it has become popular to model the optical properties of opal-like structures in terms of an effective periodically multilayered structure where the corresponding effective parameters are direction and polarization dependent. Indeed, this model could successfully explain the angular

dispersion of diffraction resonances in opal crystals, except for directions that correspond to the case of multiple-band diffraction where avoided band crossings take place.[12,13] The polarization anisotropy of diffracted light from opal crystals has also been addressed.[14–16] However, the critical angle of diffraction from opal structures has been investigated only once.[15] The corresponding experiment has been based on a system where an opal structure has been immersed in an index-matching liquid. As alluded to above, the optical properties of PhC samples with an "empty lattice" (immersed in an index-matched liquid) are expected to be qualitatively (and quantitatively) rather different from those where the PhC samples are surrounded by homogeneous materials that exhibit sizable (effective) RI contrasts.[17] Explanation of polarization anisotropies in opal colloidal crystal exclusively rely on the concept of independent light diffraction at different crystal planes.[18,19] However, the validity of this (simple and thus appealing) model has never been fully established or examined.

How far one can exploit the analogy of 3D PhCs to periodically multilayered dielectric structures when interpreting the polarization anisotropies, thus remains an open question. In particular, the fact that the critical angle of diffraction appears in the vicinity of avoided band crossings allows us to utilize this phenomenon as a sensitive probe regarding the applicability of the effective multilayered model.

In this work, we analyze polarization anisotropies in thin-film crystals of closely packed colloidal spheres. In particular, we have studied polarization anisotropies of the diffraction at crystal planes that are parallel to the films. Our crystals represent typical examples of realistic 3D PhCs with moderate refractive index contrast of about 1.5:1 that also contain different degrees of fabrication disorder. This disorder and the finite thickness of the film affect the polarization anisotropy that occurs in such crystals so that we may utilize polarization anisotropy as a sensitive probe. Therefore, we first "construct" an ideal reference sample by numerically simulating the reflectance spectra of thin-film colloidal crystals that consist of a perfectly ordered face-centered-cubic (fcc) lattice of spheres. We emphasize that we do not model realistic crystal structures numerically, but that we instead, are interested in the optical response of an ideal thin-film crystal for comparison with experimental data from real systems. The corresponding experimentally studied structures include self-assembled thin-film opal samples and force-assembled Langmuir-Blodgett (LB) crystals[20,21] that exhibit lower degrees of ordering. While opal structures represent weakly disordered fcc lattices of spheres [Figs. 1(a) and 1(b)], the LB crystals might be considered as moderately disordered systems with an underlying hexagonal symmetry [Figs. 1(c) and 1(d)]. As a result, this approach allows us to assess the polarization anisotropy as it results from, on the one hand, the disorder-induced additional light scattering, and, on the other hand, the spatial anisotropy in 3D lattice arrangements. In particular, we focus our attention on the link between the critical angle of diffraction and possible mechanisms of light depolarization in 3D lattices.

II. EXPERIMENTAL TECHNIQUE

The only way to learn about the polarization properties of ideal colloidal crystals samples with perfectly ordered lattice and identical spheres is to perform numerical simulations of their optical spectra. Therefore, we have computed angle- and frequency-resolved reflectance spectra of an ideal fcc arrangement of 25 monolayers of monodisperse spheres (RI of 1.489) that are stacked along the cubic body diagonal (the

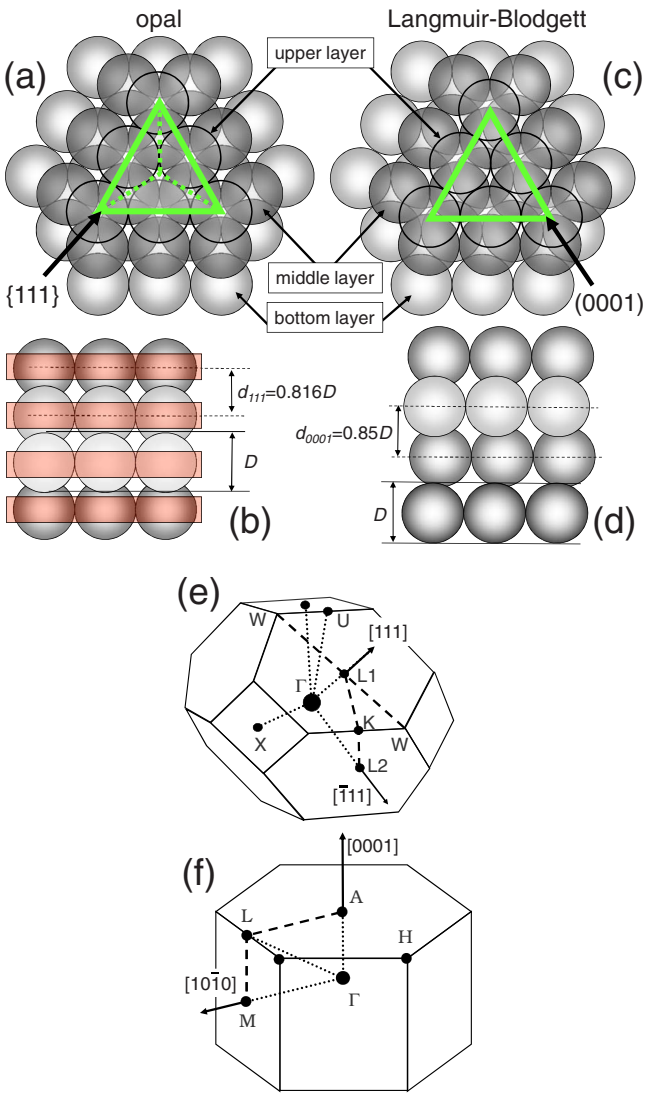

FIG. 1. (Color online) Geometry of packed spheres arranged in fcc lattices or Langmuir-Blodgett crystals. (a) A section of a fcc lattice of spheres viewed along the cubic body diagonal. The triangles denote planes of the {111} family where each (111) plane corresponds to a hexagonally close packed lattice of spheres with diameter D. (b) A section of a fcc lattice of spheres viewed along one of the cubic axes. The spacing of the hexagonally closed packed planes is denoted by d_{111}. (c) A section of a Langmuir-Blodgett (LB) crystal that consists of three (0001) planes viewed along the stacking direction. These hexagonally close packed (0001) planes of spheres are identical to the (111) planes of the fcc lattice but different planes are randomly shifted in lateral direction. (d) A section of a LB crystal viewed perpendicular to the stacking direction. The effective (0001) plane space is denoted by d_{0001}. (e) The Brillouin zone of the fcc lattice. (f) The Brillouin zone of the hexagonal lattice. Miller indices in (e) and (f) denote characteristic directions that correspond to lattice plane vectors in real space. Dash lines show the scanning directions.

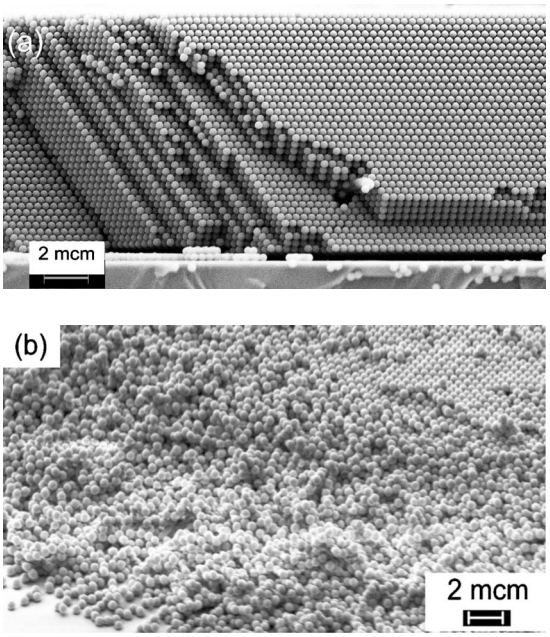

FIG. 2. (a) The SEM image of the cross section of the opal film assembled from 368 nm PMMA beads. (b) The SEM image of the cleaved LB film assembled from the 519 nm silica beads.

[111] direction) and are deposited on a glass substrate [Figs. 1(a) and 1(b)]. These computation have been performed via the so-called Fourier-modal method[22] and we have checked that a spatial discretization of 15 nm in stacking direction and 197 Fourier modes laterally lead to converged results within the linewidths of our plots. By varying the incidence angle of the incoming plane wave relative to this stack, we have obtained spectra for directions that correspond to the LKL′ and LW lines on the surface of the fcc Brillouin zone [see Fig. 1(e)]. In what follows we will refer to these reference simulations of an ideal structure simply as the "fcc sample."

Regarding actual 3D PhC samples, we have crystallized opal films in the meniscus on hydrophilic glass slides that are vertically moving up and off a suspension of poly-methyl methacrylate (PMMA) spheres [Fig. 2(a)].[23] Spheres with hydrophilic anionic surface with a RI $n_{\mathrm{PMMA}}=1.489$ and diameter $D=368$ nm (standard deviation of 8 nm) have been purchased from Microparticles GmbH. Samples of 25 $\times 20$ mm^2 size were prepared.

Improvements of the crystal structure have been achieved by applying the acoustic-noise-agitation technique to the colloidal suspension during the crystallization of the film. Details of this technique are given elsewhere.[10,24] No sintering or other means of consolidating have been applied to the prepared samples. As a result, the spherical shape of the beads in the opal is preserved and further distortions of the lattice symmetry are avoided. The ordering of prepared opals was thoroughly characterized using Fourier-transform analysis[10] and position correlation analysis[24] of the sphere arrangements in scanning electron microscopy (SEM) images. Optical diffraction of these samples was studied as a function of the angle of incidence and the azimuthal orientation of the plane of light incidence. Based on fitting the dispersion of diffraction resonances to the Bragg law projections for the fcc lattice of touching spheres, we concluded that the opal lattice contains stacking faults. In contrast, the lattice strain was largely removed due to the acoustic agitation technique mentioned above.[10] Since the opal lattice closely resembles the ideal fcc lattice [see Figs. 1(a) and 1(b)], we label the diffraction resonances according to the Miller indices associated with the corresponding fcc lattice planes. The main resonance of our interest relates to the diffraction at (111) planes, each of these planes consists of a hexagonal lattice of touching spheres that is oriented parallel to the substrate.

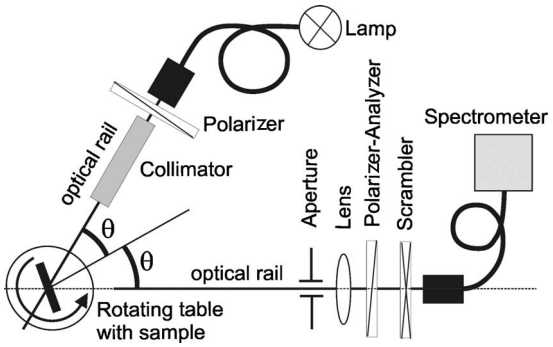

FIG. 3. Scheme of the reflectance measurement setup.

Further, we have prepared LB films by one-by-one stacking of precrystallized monolayers of SiO_2 spheres[21] that exhibit a RI $n_{\mathrm{SiO_2}}\approx 1.42$ and diameter $D=519$ nm (standard deviation of 20 nm, purchased from Microparticles GmbH). Similar to the opal films, the spheres in each monolayer crystallize into a hexagonal lattice. However, in the LB crystal these monolayers are laterally misaligned in a random fashion relative to the positions of an fcc lattice so that the LB samples can be considered as moderately disordered crystals[25] [see Figs. 1(c) and 1(d) and Fig. 2(b)]. Since one of the limits of fully ordered LB crystal is the hexagonal lattice [Fig. 1(f)], we will subsequently use the four-digit Miller index notations for this lattice, simply in order to easily distinguish between the resonances in opal and LB crystal films. Consequently, we denote the growth plane of the LB crystal films as the (0001) plane and we have studied films that consist of ten (0001) layers which have been obtained from ten deposition cycles. The standard sample size was 25 $\times 75$ mm^2. No sintering of the LB crystal films has been applied.

The angle- and frequency-resolved reflectance spectra were acquired with an angular resolution of less than 1°. The incidence angle θ was varied from 10° to 80° at steps of 2° with respect to the film normal with an uncertainty of ~0.2° (Fig. 3). This angular resolution was achieved by placing the sample at a distance of 500 nm from the collecting optics and by using an aperture to reduce the beam width (Fig. 3). Collinear-oriented polarizers were used to select the copolarized reflected light either within the plane of incidence (p polarization) or orthogonal to that plane (s polarization). High-sensitivity Peltier-cooled fixed-grating charge coupled device (CCD)-based spectrometers from Ocean Optics with a 16-bit dynamic range were used to acquire reflectance spec-

tra. Such dynamic range allows to record the signal with intensity variation of 4 orders of magnitude without substantial influence of noise providing that the dark readings amounts to 1–2 counts. Absolute values of reflectance were obtained with respect to the reference channel that includes all optical elements except for the sample. Averaging over 20 spectra at each angle was used to reduce the relative measurement error. The ~0.4 nm wavelength resolution of the spectrometer and the absence of sharp peaks in the spectra encouraged us to average the intensity readings over a 3-nm-wide range and, thus, to further reduce the uncertainty in magnitude readings to about 2×10^{-2} of a percent. Furthermore, we have employed a polarization scrambler plate in front of the light collecting optical fiber in order to avoid the polarization response of the spectrometer grating.

Similarly, spectra of cross-polarized reflected light have been obtained by turning the analyzer by 90°. In order to provide the required increase in the signal integration time, we introduced a 0.025 gray filter into the reference channel and corresponding corrections for the nonlinearity of the CCD sensitivity were used in the signal channel. However, the corresponding 40-times higher sensitivity is achieved at the cost of a threefold times increase in the dark reading so that the lower limit of the absolute values of the measured signals is $2\times10^{-5}-3\times10^{-5}$ percent.

In the applied measurement scheme (Fig. 3), the sampled volume of the crystal increases with increasing incidence angle because the spot size of nominally 1 mm in diameter for normal incidence that illuminates the sample becomes about three times larger at an incidence angle of $\theta=70°$. Further, the uncertainty in detector readings becomes larger for larger incidence angles for two reasons. First, mirror reflectance at the sample surface increases for larger incidence angles. This effect is additive to the magnitude of the diffraction resonance and, to a first approximation, does not depend on the wavelength. Consequently, when determining the polarization anisotropy of the diffraction resonances at each incidence angle, we have subtracted the magnitude of the off-resonance reflectance magnitude from the values of the backdiffracted light. A second effect is the possible inhomogeneity of the crystal lattice that may result from inhomogeneous convective liquid flow in the crystallization vessel. This can lead to additional smearing out of resonances for larger incidence angles. To reduce the influence of this factor, we have (i) performed the measurements in the central part of the samples where structural inhomogeneities are expected to be minimal and (ii) checked that the spectra in the measured area are consistent for different spot sizes at fixed incidence angle.

Once more, we want to emphasize that the numerically calculated spectra of the ideal fcc lattice are free from experimental uncertainties and any effects related to structural defects. Therefore, these calculations serve as an ideal reference sample.

In order to facilitate the comparison between the different samples as well as between samples and the ideal fcc lattice, we subsequently plot all spectra as a function of the reduced frequency that is measured in dimensionless units D/λ. Finally, unless explicitly stated otherwise, we subsequently consider only copolarized reflection spectra into the zeroth order, i.e., the reflection is measured for the same polarization as the incident (linearly polarized) light. In this case, it suffices to specify the polarization of the incident light alone, i.e., p(111) denote the copolarized reflectance peak associated with the (111) plane under *p*-polarized incidence.

In the case of an opal film, we have identified the orientation of the plane of the incident light by using the surface diffraction pattern. A corresponding fit of the Bragg law to the experimentally obtained angle dispersion of the (111) resonances yields an interplane distance of $d_{111}=301$ nm (so that $d_{111}/D=0.816$) and an effective long wavelength RI $n_{eff}=1.361$.[10] In addition, from the periodicity of the Fabry-Perot oscillations in the reflectance spectra and the effective RI in the long-wavelength limit, we have determined the thickness of the film to be 25 (111) planes—and this is the reason why we have computed the reference reflectance spectra for the fcc lattice for 25 monolayers. A similar fit of the (0001) diffraction resonance for the LB film delivers the a lattice plane spacing $d_{0001}=441$ nm (so that $d_{0001}/D=0.85$), and an effective long wavelength RI $n_{eff}=1.245$.[26] These results provide clear evidence of the expected lower volume fraction of spheres in the LB crystal film as compared to the dense packed fcc and opal lattices.

III. POLARIZATION ANISOTROPY OF DIFFRACTION RESONANCES

In Figs. 4(a) and 4(b), we present numerically calculated reflectance spectra of the thin-film fcc sample under *s*- and *p*-polarized illumination for the LKL′ scanning direction. These spectra contain two resonances that are assigned to (111) and $(\bar{1}11)$ planes. In what follows, we will focus on three important angles of incidence that we have indicated by A, B, and C.

The A direction corresponds to an avoided crossing in the resonance dispersion [Fig. 4(a)] and is observed in the reflectance spectra under *s*-polarized incident light. The characteristic feature of the A direction is the coexistence of $s(111)$ and $s(\bar{1}11)$ resonances at $D/\lambda=0.535$ and 0.572. In order to obtain the magnitude of the diffraction resonance, ΔR, in a uniform manner for all samples, we have measured the height of the resonance peak and have subtracted the background to obtain $\Delta R=R_{\max}-R_{0.37}$. Here, we have measured the background value $R_{0.37}$ at $D/\lambda=0.37$ which lies below the (111) resonance. As shown in Fig. 4(c), the magnitudes of $s(111)$ and $s(\bar{1}11)$ resonances are rather similar at $\theta_A=54°$. In contrast, p(111) and $p(\bar{1}11)$ cross each other at the same A angle at $D/\lambda=0.549$ [Fig. 4(b)], i.e., in between two *s* bands. Furthermore, the value of the *p*-band peak is about half of that of *s* bands [Fig. 4(c)].

The B direction is specific to the long-wavelength end of the spectra. Along this direction the intensity of the off-resonance reflected *p*-polarized light approaches its minimum. In other words, this is the Brewster angle [Fig. 4(b)].

The C direction is the one, along which the resonance in *p*-polarized light vanishes from the spectra of the fcc sample [Figs. 4(b) and 4(c)]. By definition, we can assign the angle $\theta=62°$ to be the critical angle of diffraction at the (111)

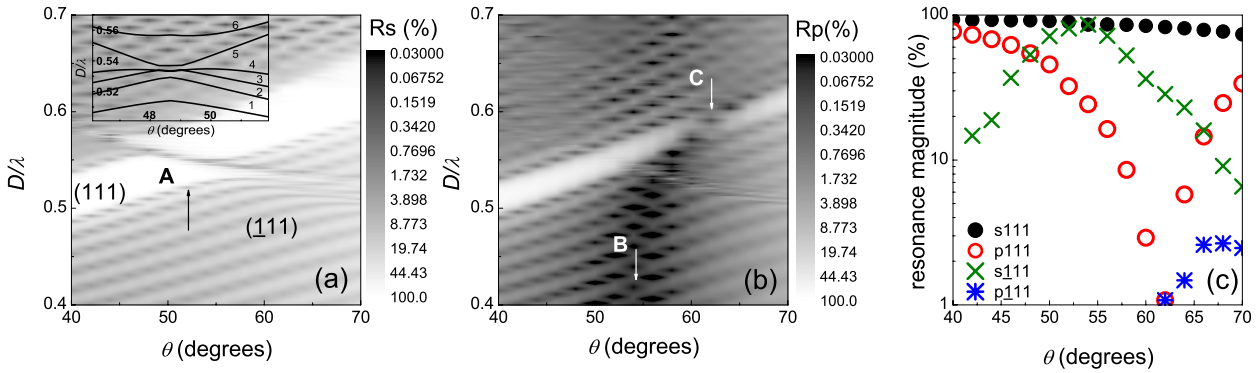

FIG. 4. (Color online) Computed angle- and wavelength-resolved copolarized reflectance spectra for 25 layers of a fcc lattice of spheres. Panels (a) and (b) depict, respectively, the case of *s*- and *p*-polarized incident light. Miller indices are used to identify the resonances associated with different crystal planes. (c) Angular variation in the magnitudes of the diffraction resonances that are indicated by arrows and letters on panels (a) and (b). The arrows A, B, and C denote, respectively, angles of the incident light that correspond to band anticrossing, Brewster and critical angle of diffraction. The inset to panel (a) shows a snapshot of the photonic band structure for the fcc lattice of touching spheres near the angle A. The corresponding Bloch modes are numbered from 1 to 6. In these and the following spectra the logarithmic grayscale coding has been chosen to emphasize the spectral features. The corresponding experimental results for an opal film are displayed in Fig. 5. See the text for further details.

planes. At higher angles of incidence, this resonance is restored and, moreover, it is then accompanied by the p($\bar{1}11$) resonance [Fig. 4(c)].

The reflectance spectra of the real-life opal film show similar diffraction resonances for the (111) and ($\bar{1}11$) planes as those discussed in the ideal fcc lattice [see Figs. 5(a) and 5(b)]. Near the incidence angle $\theta_A \approx 50°$, the band anticrossing separates the *s*-polarized resonance into two bands that are centered at $D/\lambda=0.523$ and 0.554, respectively [see Fig. 5(a)]. Along the same A direction, the p(111) resonance appears at $D/\lambda=0.541$. In this region of band splitting, the value associated with the *s*($\bar{1}11$) resonance reaches the value associated with the *s*(111) resonance, again very similar to the situation in the ideal fcc lattice discussed above (see Figs. 4 and 5).

At angles $\theta=54°-56°$, both, the intensities of the off-resonant reflectance and the p(111) resonance are reduced by two orders of magnitude and reach a minimum [see Fig. 5(b)]. However, in contrast to the fcc sample the diffraction peak does not collapse [Fig. 5(c)]. At higher angles, both peak and background reflectance recover their intensity. Interestingly, at $\theta=62°$ the p(111) resonance does not exhibit any peculiarities.

The reflectance patterns of the LB crystal film contain one strong resonance band in both polarizations [see Figs. 6(a) and 6(b)]. Under *p*-polarized illumination both, the resonance and off-resonance reflectance intensity, display a minimum at $\theta=52°$.

The distinctive feature of the p resonance in the LB crystal film is its nonmonotonous angular dispersion. In fact, within the $\theta=48°-56°$ angle range, the p(0001) resonance is substituted by another resonance that exhibits the opposite dispersion [Fig. 6(b)]. This effect looks like a kink in the resonance dispersion. By analogy to opals, we associate this behavior to the avoided crossing of the p(0001) and p($\bar{1}11$) diffraction branches. The fact that anticrossing appears in the spectra of *p*-polarized light can be associated with the specific symmetry of the LB crystal film. Despite the poorly defined anticrossing, the frequency splitting between *p* and *s*

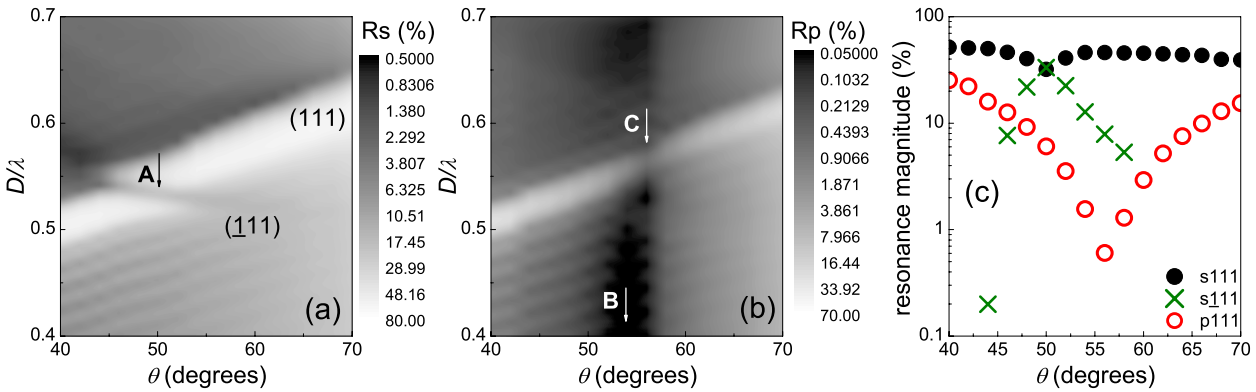

FIG. 5. (Color online) Measured angle- and frequency-resolved copolarized reflectance spectra from 25 layers of an opal film. Panels (a) and (b) depict, respectively, the case of *s*- and *p*-polarized incident light. Miller indices are used to identify the resonances associated with different crystal planes. (c) Angular variation in the magnitudes of the diffraction resonances. The arrows A, B, and C denote angles similarly to those in Fig. 4. The corresponding theoretical results for an ideal structure are displayed in Fig. 4. See the text for further details.

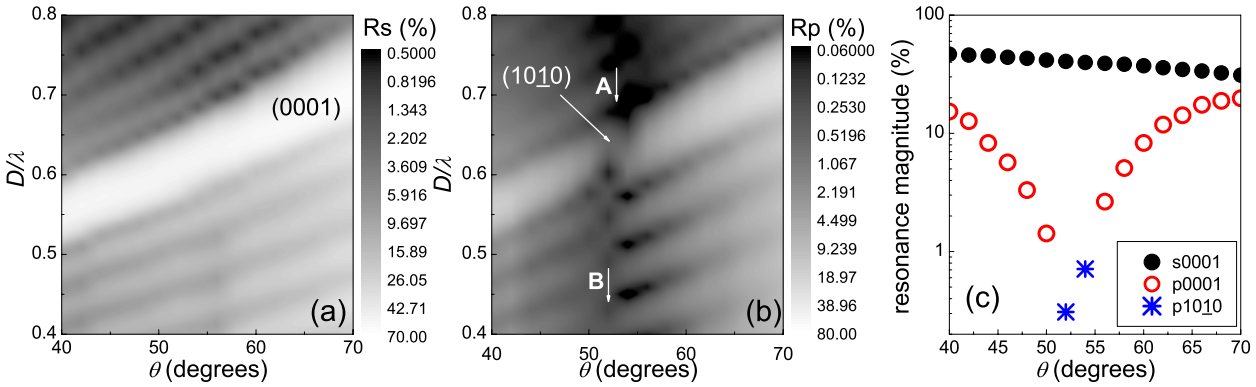

FIG. 6. (Color online) Measured angle- and frequency resolved copolarized reflectance spectra from ten layers of a LB crystal film. Panels (a) and (b) depict, respectively, the case of *s*- and *p*-polarized incident light. Miller indices for a hexagonal lattice are used to identify the resonances associated with different crystal planes. (c) Angular variation in the magnitudes of the diffraction resonances. The arrows A and B denote angles similarly to those in Fig. 4. See the text for further details.

bands is about $\Delta(D/\lambda)=0.023$ which is just a little lower as compared to the corresponding shift that we have observed in the opal. Thus, in the LB crystal film the A, B, and C characteristic directions of the fcc sample merge into one single direction.

The angular diagrams of the polarization anisotropy of diffraction resonances in our PhC films are represented by the ratio R_p/R_s for the (111) resonance reflectance (see Fig. 7; recall that by R_p and R_s we denote the copolarized reflectance spectra, i.e., R_p corresponds to *p*-polarized backscattered light under *p*-polarized incidence and R_s corresponds to *s*-polarized backscattered light under *s*-polarized incidence). If the corresponding resonance cannot be resolved in the spectrum, we have substituted its value by the value of the reflectance at the projected resonance frequency. The diagram for the fcc sample shows a sharp minimum at $\theta_c=62°$ [curve 1, Fig. 7(a)]. In this sample, the R_p/R_s ratio for the off-resonance reflectance at $D/\lambda=0.37$ shows an even deeper minimum at $\theta_B\approx 56°$ [curve 2, Fig. 7(a)]. This latter angle corresponds to the Brewster angle $\theta_B=\arctan(n_{eff})=54°$ in the ideal fcc lattice with an effective RI $n_{eff}\approx\sqrt{0.74n_{\mathrm{PMMA}}^2+0.26}=1.379$ that is given by the ideal fcc volume packing fraction of 0.74. The inaccuracy of the Brewster angle estimate originates from the poor approximation of the effective index by this simple formula. It is instructive to mention that curve 1 represents anisotropy values that are related to different frequencies, whereas curve 2 corresponds to the anisotropy at fixed frequency.

The polarization anisotropy of the opal film largely follows the behavior of the ideal fcc lattice but with the (111) resonance anisotropy maximum at $\theta=56°$ [see Fig. 7(b)]. The corresponding Brewster angle for the low frequency off-resonance reflectance is $\theta_B\approx 54°$. It coincides with our estimate of the Brewster angle when we take as the effective RI $n_{eff}=1.361$ which we have obtained from the Bragg fit to the $s(111)$ resonance dispersion. Thus and rather surprisingly, the direction of the (111) resonance anisotropy maximum differs only marginally from the Brewster angle.

This tendency is supported by the anisotropy diagrams of the LB crystal film. In this case, the minimum of the R_p/R_s diagram for the (0001) diffraction resonances cannot be resolved due to the anticrossing with the (10$\bar{1}$0) band discussed above. However, the off-resonance anisotropy at $D/\lambda=0.37$ peaks at the angle $\theta_B=52°$ [see Fig. 7(c)]. This Brewster angle estimate $\theta_B=51.2°$ is consistent with the estimate for the LB crystal film that uses the effective RI n_{eff}

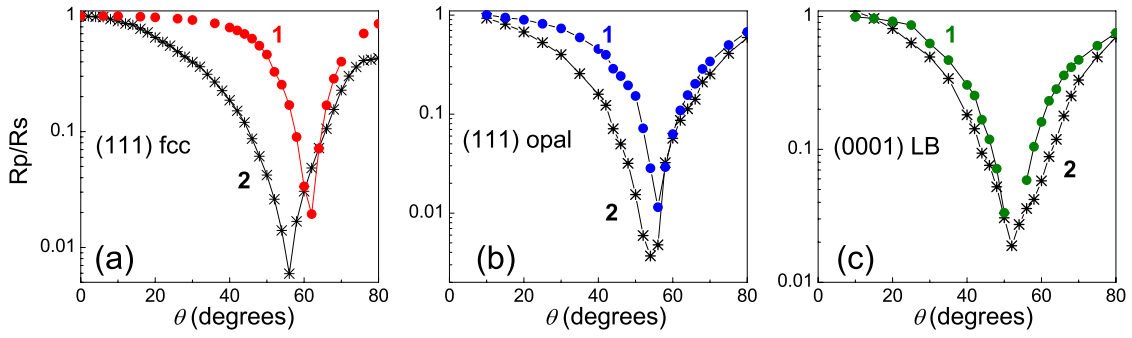

FIG. 7. (Color online) Angular variation in the polarization anisotropy in copolarized reflectances that are associated with the (111) diffraction resonance in the case of ideal fcc lattice: [panel (a), curve "1:" solid line with dots] and opal film [panel (b), curve 1: solid line with dots] and the corresponding (0001) diffraction resonance in the case of LB crystal film [panel (c), curve 1: solid line with dots]. The anisotropy is represented in the form of R_p/R_s, where R_p and R_s, respectively, denote copolarized reflectance for *p*- and *s*-polarized incident light. For comparison, each panel also features the results for off-resonant cases at $D/\lambda=0.37$ (curves "2" in all panels: solid lines with crosses). See the text for further details.

=1.245 which we have extracted from the Bragg fit to the $s(0001)$ resonance dispersion. The smaller value as compared to that of the opal film is consistent with the lower volume fraction of the high-dielectric material (the spheres) in the LB crystal film.

IV. ONE-DIMENSIONAL MULTILAYER MODELS

The dispersion of diffraction resonances in colloidal crystals that are stabilized by electrostatic forces in a liquid is well described by expanding diffraction in a 3D lattice into a series of resonances from one-dimensional (1D) lattices.[11] A similar approach also works satisfactorily in the case of close-packed opal-like structures that are impregnated by an index-matching liquid and—albeit to lesser degree—in the case of these structures with moderate RI contrasts.[13] This observation makes it reasonable to check if the 1D approach can also be used to interpret the polarization anisotropy of our samples.

Let us apply the model of an effectively periodic multilayered structure to the ideal fcc lattice. In the simple Bragg-mirror-type model, the critical angle of diffraction can be expressed as[27]

$$\tan\theta_c = \sqrt{\frac{\varepsilon_a\varepsilon_b}{(\varepsilon_a+\varepsilon_b)\varepsilon_v - \varepsilon_a\varepsilon_b}}, \tag{1}$$

where ε_a, ε_b, and ε_v denote, respectively, the dielectric constants of the materials in layers a, layers b, and the external medium v. In order to apply this expression to an fcc lattice of spheres stacked along the [111] direction one has to determine the (effective) modulation of a dielectric constant profile along the [111] axis [see Fig. 1(b)]. Taking the modulation depth as ~60% (Ref. 28) for the ideal fcc lattice, the critical angle $\theta_c=62°$ from Fig. 4(a) and $\varepsilon_v=1$ for air, we derive effective dielectric constants of layers $\varepsilon_a=2.08$ and $\varepsilon_b=1.25$, respectively. Since the effective dielectric constant of the ideal fcc lattice that is assembled from PMMA spheres is about $\varepsilon_{eff}=f_{sphere}\varepsilon_{\mathrm{PMMA}}+f_v\varepsilon_v=1.88$, where $f_{sphere}=0.74$ and $\varepsilon_v=1$ for air, we can estimate the fraction, f_a, of a layers in the resulting effective Bragg stack $\varepsilon_{eff}=f_a\varepsilon_a+(1-f_a)\varepsilon_b$ as $f_a=0.76$. If we, similarly, assume $\theta_c=56°$ to be the critical angle of diffraction in the real-life opal film, we have to adopt $\varepsilon_a=2.187$ and $\varepsilon_b=1$ in order to satisfy the expression (1). This raises the important question whether we at all can assume that the depth of dielectric constant modulation in slightly disordered fcc lattice is 100%. Clearly, this is impossible, because from an SEM inspection of the samples and the above-mentioned Bragg fit to the angular dispersion of the (111) resonance, we have found $d_{111}<D$. Moreover, we simply cannot apply the above procedure of an effective 1D model to the LB crystal film because expression (1) would force us to chose $\varepsilon_b<1$.

Alternatively, the layered diffraction model that has been specifically adapted to opal structure leads to the expression for the critical angle of diffraction as $\sin\theta_c=\sqrt{\varepsilon_{eff}/(2\varepsilon_v)}$.[15] The validity of this expression has been confirmed in the case of opal films that have been immersed in an index-matching liquid. However, in the case of sizable (effective) RI contrast between opal film and the surrounding medium such as is the case for our ideal fcc lattice and the real-life opal film, this expression yields a critical angle $\theta_c=74°$ which far exceeds the value $\theta_c=62°$ that we have observed in the copolarized calculated reflection spectra under p-polarized illumination (see Fig. 5).

The failure of the effective 1D models to describe our computational and experimental findings leads us to consider more carefully various physical mechanisms that may contribute to the depolarization phenomena described in Sec. III.

V. LIGHT DEPOLARIZATION IN COLLOIDAL PHOTONIC CRYSTALS

A. Lattice disorder

The collapse of the resonance under p-polarized illumination when approaching the critical angle of diffraction is manifest not only as a decrease in the value on resonance but also as a narrowing of its linewidth. Both of these requirements are fulfilled at $\theta_c=62°$ in the case when the ideal fcc lattice is scanned along the LKL line of the Brillouin zone [see Fig. 8(a)]. In the case of the real-life opal film, the resonance values achieve their minimum at $\theta=56°$ but the resonance bandwidth remains at 60% of its value at $\theta=10°$ [see Fig. 8(b)]. In the case of the LB crystal film, we observe qualitatively the same omnipresence of the diffraction resonance in the p-polarized light as for the opal film [see Fig. 8(c)].

The obvious difference between the ideal fcc lattice and the experimentally prepared samples is the fabrication disorder of the latter. Obviously, the lattice disorder is accompanied by random scattering processes that are known to give rise to depolarization effects.[29] More precisely, random scattering could be able to prevent the resonance under p-polarized illumination from strong narrowing and vanishing.

It is commonly accepted[30] that defects in the opal lattice are responsible for a reduction of the magnitude of the diffracted light intensity by about a factor of two as compared to the values of ideal fcc lattices. This decrease for (111) diffraction along the plane normal is solely the result of disorder that diverts a fraction of the light flow in the resonance order from the expected scattering direction, the peak intensity provides an effective or average measure of losses that are caused by imperfect periodicity in a stacking sequence of (111) planes [cf. spectra in Figs. 8(a) and 8(b)]. On the other hand, the almost twofold increase in the relative full peak width at half maximum (FWHM) $\Delta E/E_{center}$ at $\theta\approx 10°$ in the LB film relative to the opal film together with an almost unchanged peak magnitude [cf. Figs. 8(b) and 8(c)] can be attributed to the stronger light localization in a partly disordered lattice.[31] Although we have found a substantially increased disorder in the LB crystal relative to the opal film (cf. Figs. 2 and 8), there is no corresponding difference in magnitude of the diffraction resonance [see Figs. 8(b) and 8(c)]. Moreover, while random scattering can certainly lead to a smearing out of the polarization anisotropy, it is difficult to conceive that it will be able to completely suppress the critical angle of diffraction. Therefore, we have to examine

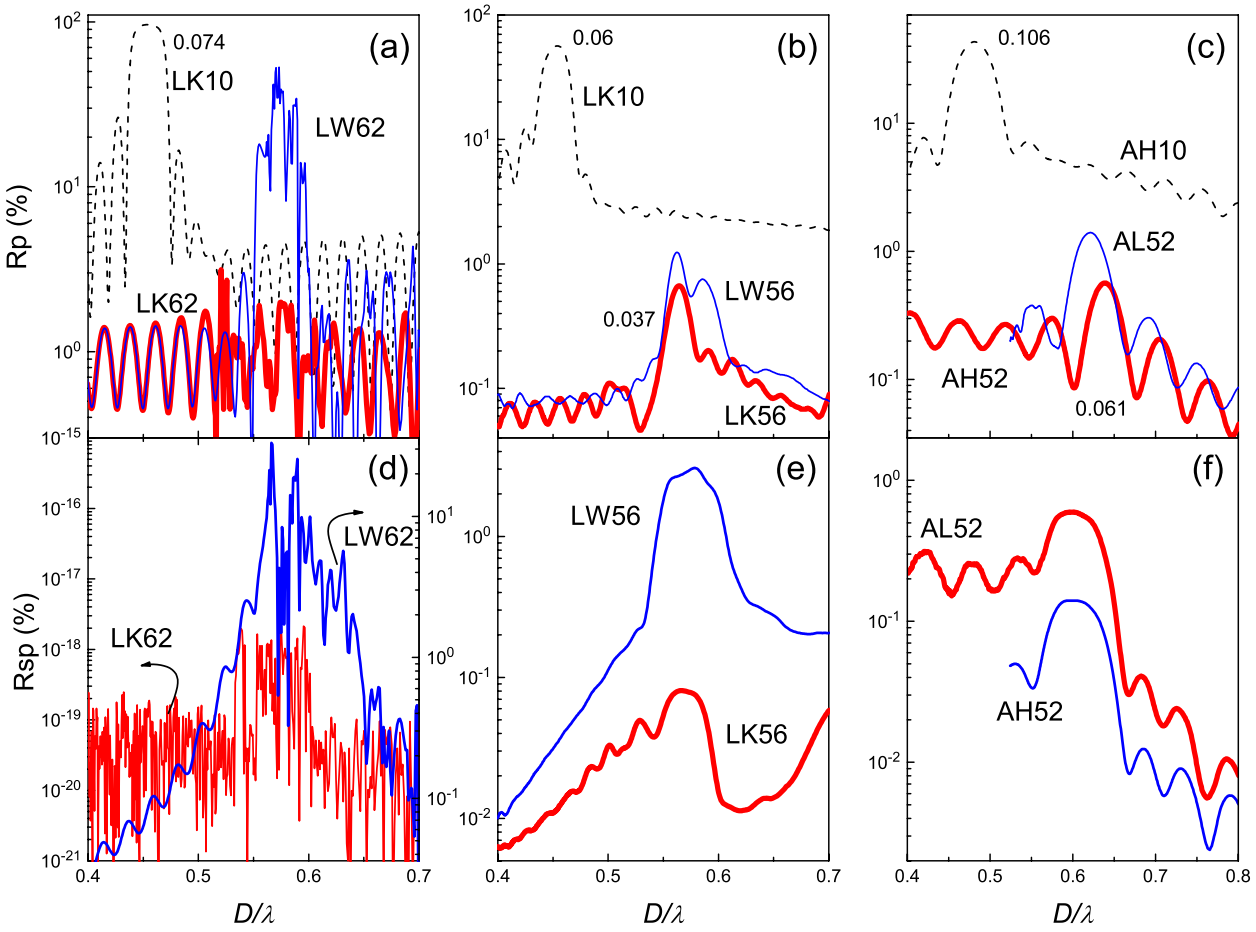

FIG. 8. (Color online) Copolarized [(a), (b), and (c)] and cross-polarized [(d), (e), and (f)] reflectance for *p*-polarized illumination for the ideal fcc-stacked, opal, and LB crystal films under various angles θ relative to the normal. (a) copolarized reflectance spectra of the ideal fcc-stacked film for *p*-polarized illumination along the LKL line in the BZ (see Fig. 1) for $\theta=10°$ and $\theta=62°$ (dashed and bold solid line, respectively) and along the LW line in the BZ [see Fig. 1(e)] for $\theta=62°$ (thin solid line). The number at the peak of the LKL spectra for $\theta=10°$ denotes its relative FWHM. (b), (c) the same as (a) for the opal film ($\theta=10°$ and $\theta=56°$) and the LB crystal film ($\theta=10°$ and $\theta=52°$). For the LB crystal film, the 30° azimuth rotation of the sample relates to changing the scanning direction from the AL to the AH line, which are both high-symmetry lines within the BZ zone [see Fig. 1(f)]. However, this difference is irrelevant in the case of a LB film due to the disorder in these structures. (d) cross-polarized reflectance for the ideal fcc-stacked film along the LKL and LW directions in the BZ and for an illumination angle $\theta=62°$. (e), (f) the same as (d) for the opal film ($\theta=56°$) and the LB crystal film ($\theta=52°$). See the text for further details.

further mechanisms that could contribute to the observed loss of the critical angle of diffraction in real-life 3D PhCs.

B. Resonance vs off-resonance polarization anisotropy

It is rather instructive to consider the entire angle- and frequency-resolved polarization anisotropy map. Specifically, when comparing the polarization anisotropy spectra along the LKL scanning direction at frequencies below and above the (111) or (0001) resonance (see Fig. 9), we notice that, at the Brewster angle, the polarization anisotropy of the off-resonance reflectance exceeds by a factor of three that at the frequencies above the (111) or (0001) resonance. We illustrate this fact by depicting in Fig. 9 the polarization anisotropy spectra for the angles A and C. Thus, the polarization anisotropy in the effective medium regime of light propagation is stronger than in the regime in which the light is coupled to eigenmodes of the PhC.

In the range of the (111) resonance, the polarization anisotropy is further reduced relative to its off-resonance value. This difference is particularly pronounced in the ideal fcc lattice—the (111) backdiffracted light is about an order of magnitude less polarized than the off-resonance reflected light [see Fig. 9(a)]. Low values of the polarization anisotropy remain noticeable in the (111) resonance of the opal film but this effect almost completely vanishes for the (0001) resonance of the LB crystal film [see Figs. 9(b) and 9(c)]. The only exception to this is the anisotropy for angle C in the ideal fcc lattice. In view of the fact that the low-frequency off-resonance polarization anisotropy solely relates to the light reflection at the film-air interface, we associate this reduction of the polarization anisotropy to rather inefficient light coupling to PhC eigenmodes at the air-PhC interface. Within the resonance bandwidth only evanescently decaying or inhomogeneously propagating modes are available for coupling, hence the light of both polarizations is strongly

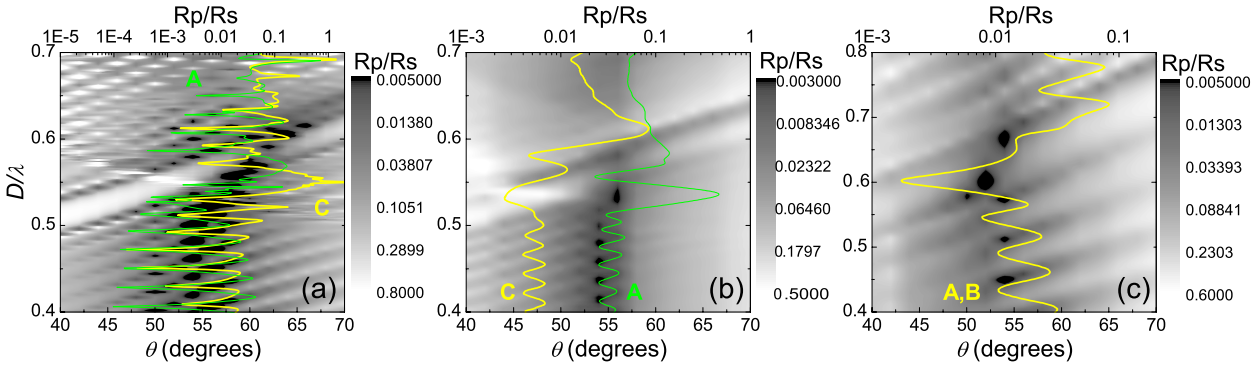

FIG. 9. (Color online) Angle- and frequency-resolved polarization anisotropy spectra along the LKL direction for (a) the ideal fcc lattice, (b) the opal film, and (c) the LB crystal film. Overlayed are the polarization anisotropy spectra for the angles A (thin solid line) and C (thick solid line) and the corresponding values are indicated on the top horizontal edge. See the text for further details.

reflected which leads to a significant reduction in the polarization anisotropy.

Since lattice defects introduce a continuum of defect modes that may allow light to flow through a PhC in the spectral range of a stop band, they also may contribute to the increase in the resonance polarization anisotropy in disordered PhCs. For instance, the resonance and off-resonance anisotropy in the LB crystal film are very similar at nearly all angles except for those in the neighborhood of the Brewster angle (see Fig. 9).

Furthermore, for the ideal fcc lattice, we notice a pronounced feature in the polarization anisotropy in the range of the (111) and ($\bar{1}$11) resonance anticrossing, i.e., for angles between 50° and 55° and frequencies near $D/\lambda=0.55$ [see Fig. 9(a)]. In fact, in this range the breakdown of polarization anisotropy takes place, i.e., the reflection coefficients for the *p*- and *s*-polarized light take on the same values. For the opal film, we observe a similar breakdown of the polarization anisotropy near the band anticrossing at $\theta=46-52°$. If we take into account that PhC modes are indistinguishable in the anticrossing range [inset, Fig. 4(a)], this breakdown of the polarization anisotropy corresponds to the simultaneous excitation of all existing modes independent of their symmetry.

C. Band anticrossing vs diffraction polarization anisotropy

Azimuthal rotation of the plane of light incidence with respect to the opal lattice by 30° results in a strong change in the appearance and dispersion of diffraction resonances in both numerically and experimentally (see also Ref. 10) obtained spectra. This rotation corresponds to a change from the LKL to the LW scanning direction [see Fig. 1(e)]. However, this azimuthal rotation leads to a strong increase in the resonance magnitude for *p*-polarized illumination in the ideal fcc lattice at $\theta=62°$ [see Fig. 8(a)] whereas the same rotation produces small changes in the resonance magnitude for the opal crystal film [see Fig. 8(b)]. This pronounced difference between ideal fcc crystal and opal films is a consequence of a fabrication disorder associated with the opal films. This spatial anisotropy is the key observation for the explanation of the complex depolarization behavior of our samples.

The absence of the decay of the *p*-polarized resonance when scanning along the LW line (as opposed to scanning along the LK line) leads to the modification of the polarization anisotropy of the ideal fcc lattice and the opal film (see Fig. 10). At frequencies below the (111) resonance, the anisotropy achieves it maximum at the Brewster angle in the same manner as along LK direction. However, the anticrossing of the LW dispersions of the (111), (200), and ($\bar{1}$11) diffraction resonances is shifted toward the Brewster angle so that the anticrossing ranges include angle C. As a result, the breakdown of the polarization anisotropy replaces the critical angle of diffraction. We thus obtain that the band mixing in the anticrossing range suppresses the polarization anisotropy.

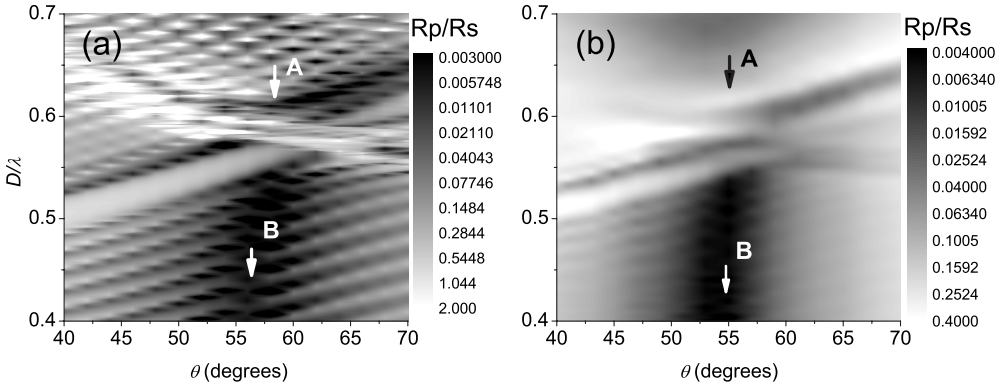

FIG. 10. Angle- and frequency-resolved polarization anisotropy spectra along the LW direction for (a) the ideal fcc lattice and (b) the opal film. The arrows indicate angles A and B. See the text for further details.

The fact that the critical angle of diffraction in 3D crystals becomes a function of the azimuthal orientation of the plane of light incidence establishes the failure of effective 1D multilayered structure models for the interpretation of the polarization anisotropy of diffraction resonances in 3D PhCs.

D. Cross-polarization coupling

An efficient mechanism that leads to a direction-dependent suppression of the critical angle of diffraction in 3D lattices is the *s*-*p* polarization conversion. For scanning along the LW line the numerical simulations show the high efficiency of polarization mixing that occurs over a broad spectral range around the direction A [see Fig. 8(d)]. At the nominal critical angle, up to 30% of incoming *s*-polarized light gets scattered into *p*-polarized light. Hence, the cross-polarization scattering provides a further mechanism for washing out the critical angle of dispersion. Importantly, for the LK scanning direction, cross-polarization coupling in ideal fcc lattice becomes at least 10^{20} times weaker. This observation explains the strong directionality of the critical angle of diffraction. In the experimentally realized structures, we find that the cross-polarization contribution is much weaker—up to 3% along LW direction at $\theta=56°$—but it persists for all scanning directions. In accordance with the simulation results, the cross-polarization coupling is reduced by an order of magnitude along the LK direction for the same incidence angle [see Fig. 8(e)]. It is interesting that in the poorly structured LB crystal film the cross-polarization coupling is smaller than in the opal film. We would also like to note that in all three studied colloidal crystals, the maximum of the cross-polarization coupling occurs near the diffraction resonance. The presence of lattice defects and cracks in the films is the origin for the much lower cross-polarization conversion efficiency which we observe in the experimentally prepared colloidal crystals. We will discuss the nature of the cross-polarization effects in a separate paper. At this point, we only want to mention that for a given direction of light propagation, the efficiency of the relevant process is directly related to the asymmetry of the electromagnetic field distribution within a unit cell of a PhC lattice.[9] As a result, experimentally unavoidable lattice defects represent an omnipresent source for cross-polarization effects for all directions of incidence.

Returning to the copolarized reflectance spectra of the opal film (see Fig. 5), we can now conclude that there is no specific critical angle of diffraction for the p(111) resonance. The minimum of the *p*-resonance magnitude corresponds to the light refraction at the opal-air boundary, i.e., to the Brewster angle. Its apparent shift to higher angles of incidence is a result of mixing with cross-polarized converted light. The latter component peaks in the range of the avoided band crossing that occurs in the opal at marginally smaller angles. Additionally, the azimuthal misalignments of crystallites in the opal film reduces the sharpness of the observed peak in the polarization anisotropy diagram of the p(111) backdiffracted light [see Fig. 7(b)]. A similar conclusion applies to the LB crystal film, where the polarization anisotropy of the diffraction resonance peaks at the Brewster angle due to a much weaker cross-polarization conversion [see Fig. 8(f)].

VI. SUMMARY

We have studied the polarization anisotropy of the copolarized resonantly backdiffracted and copolarized off-resonance reflected light in 3D thin-film colloidal crystals with moderate RI contrast: an ideal fcc lattice of PMMA spheres, opal crystal films with slightly disordered fcc lattices, and LB crystal films that consist of stacked, laterally misaligned but individually ordered monolayers of two-dimensional close-packed crystals of silica spheres.

In all cases, we have observed strong polarization anisotropy of a diffraction resonance from the crystal planes that are parallel to the film surface. Moreover, the value of the corresponding anisotropy is nearly the same as that at the Brewster angle which we obtain when considering these crystals as effective homogeneous media whose parameters are extracted from the low-frequency regime. Furthermore, we have demonstrated in the case of diffraction from these 3D lattices that the critical angle of diffraction cannot be uniquely defined. In fact, in order to observe a collapse of the diffraction resonance under *p*-polarized incident light, a sample should be an fcc monocrystal and the plane of incidence should include three high-symmetry axes of the fcc lattice from the $\langle 111\rangle$ and $\langle 200\rangle$ families. In this context, we have identified the two major physical mechanisms that contribute to the elimination of the critical angle of diffraction. These are the interactions of the bands in the range of avoided band crossings and the cross-polarization conversion in the case of asymmetric electromagnetic field distributions within a unit cell of the lattice. These mechanisms make the polarization anisotropy of diffraction strongly dependent on the azimuth orientation of the lattice with respect to the plane of incidence as well as upon the lattice distortion by intrinsic defects. In a view of these results, we can conclude that the polarization anisotropy of diffraction in 3D crystals with moderate refractive index contrast cannot be adequately modeled via diffraction in effective periodic multilayered structures.

ACKNOWLEDGMENTS

S.G.R. and U.P. acknowledge financial support from the DFG-Cluster of Excellence "Engineering Advanced Materials" (FAU, Germany). The research of M.B. and S.G.R. is supported by COST Action MP0702 and SFI RFP under Grant No. PHY076. S.E. and K.B. acknowledge the support by the Deutsche Forschungsgemeinschaft and the State of Baden-Württemberg through the DFG-Center for Functional Nanostructures (CFN) within project A1.1. S.E. is co-funded by Karlsruhe School of Optics & Photonics. We would like to thank Christian Wolff for carrying out the band-structure computations for the ideal fcc structure.

*Corresponding author; sergei.romanov@mpl.mpg.de

[1] J. D. Joannopoulos, S. G. Johnson, J. N. Winn, and R. D. Meade, *Photonic Crystals* (Princeton University Press, Princeton, NJ, 2008).
[2] K. Busch, G. von Freymann, S. Linden, S. F. Mingaleev, L. Tkeshelashvili, and M. Wegener, Phys. Rep. **444**, 101 (2007).
[3] A. Yariv and P. Yeh, *Propagation and Control of the Laser Radiation* (Wiley, New York, 1984).
[4] F. López-Tejeira, T. Ochiai, K. Sakoda, and J. Sánchez-Dehesa, Phys. Rev. B **65**, 195110 (2002).
[5] Y. Xia, B. Gates, Y. Yin, and Yu Lu, Adv. Mater. **12**, 693 (2000).
[6] I. I. Tarhan and G. H. Watson, Phys. Rev. Lett. **76**, 315 (1996).
[7] A. V. Baryshev, A. A. Kaplyanskii, V. A. Kosobukin, K. B. Samusev, D. E. Usvyat, and M. F. Limonov, Phys. Rev. B **70**, 113104 (2004).
[8] S. G. Romanov and C. M. Sotomayor Torres, Proc. SPIE **6182**, 61820H (2006).
[9] A. Balestreri, L. C. Andreani, and M. Agio, Phys. Rev. E **74**, 036603 (2006).
[10] W. Khunsin, G. Kocher, S. G. Romanov, and C. M. Sotomayor Torres, Adv. Funct. Mater. **18**, 2471 (2008).
[11] For descriptions of such system see, e.g., Phase Transitions **21**, Issues 2–4, 73–249 (1990).
[12] H. M. van Driel and W. L. Vos, Phys. Rev. B **62**, 9872 (2000).
[13] S. G. Romanov, T. Maka, C. M. Sotomayor Torres, M. Müller, R. Zentel, D. Cassagne, J. Manzanares-Martinez, and C. Jouanin, Phys. Rev. E **63**, 056603 (2001).
[14] J. F. Galisteo-Lopez, F. Lopez-Tejeira, S. Rubio, C. Lopez, and J. Sanchez-Dehesa, Appl. Phys. Lett. **82**, 4068 (2003).
[15] A. G. Bazhenova, A. V. Sel'kin, A. Yu. Men'shikova, and N. N. Shevchenko, Phys. Solid State **49**, 2109 (2007).
[16] S. G. Romanov, Phys. Solid State **49**, 536 (2007).
[17] M. Notomi, Phys. Rev. B **62**, 10696 (2000).
[18] A. V. Baryshev, A. B. Khanikaev, H. Uchida, M. Inoue, and M. F. Limonov, Phys. Rev. B **73**, 033103 (2006).
[19] A. V. Baryshev, A. B. Khanikaev, R. Fujikawa, H. Uchida, and M. Inoe, Phys. Rev. B **76**, 014305 (2007).
[20] S. Reculusa and S. Ravaine, Chem. Mater. **15**, 598 (2003).
[21] M. Bardosova, P. Hodge, L. Pach, M. E. Pemble, V. Smatko, R. H. Tredgold, and D. Whitehead, Thin Solid Films **437**, 276 (2003).
[22] L. Li, J. Opt. Soc. Am. A **14**, 2758 (1997).
[23] M. Müller, R. Zentel, T. Maka, S. G. Romanov, and C. M. Sotomayor Torres, Chem. Mater. **12**, 2508 (2000).
[24] A. Amann, W. Khunsin, G. Kocher, C. M. Sotomayor Torres, and E. P. O'Reilly, Proc. SPIE **6603**, 660321 (2007).
[25] S. G. Romanov, M. Bardosova, I. Povey, D. Whitehead, M. Pemble, and C. M. Sotomayor Torres, Appl. Phys. Lett. **90**, 133101 (2007).
[26] S. G. Romanov, M. Bardosova, M. Pemble, and C. M. Sotomayor Torres, Appl. Phys. Lett. **89**, 043105 (2006).
[27] A. A. Dukin, A. Feoktistov, A. V. Medvedev, A. B. Pevtsov, V. G. Golubev, and A. V. Selkin, J. Opt. A, Pure Appl. Opt. **8**, 625 (2006).
[28] G. M. Gajiev, V. G. Golubev, D. A. Kurdyukov, A. V. Medvedev, A. B. Pevtsov, A. V. Sel'kin, and V. V. Travnikov, Phys. Rev. B **72**, 205115 (2005).
[29] A. Aiello and J. P. Woerdman, Phys. Rev. Lett. **94**, 090406 (2005).
[30] A. F. Koenderink and W. L. Vos, J. Opt. Soc. Am. B **22**, 1075 (2005).
[31] T. Schwartz, G. Bartal, S. Fishman, and M. Segev, Nature (London) **446**, 52 (2007).